Insights into polythiol-assisted AgNP dissolution induced by bio-relevant molecules

Marianne Marchioni, Thomas Gallon, Isabelle Worms, Pierre-Henri Jouneau, Colette Lebrun, Giulia Veronesi, Delphine Truffier-Boutry, Elisabeth Mintz, Pascale Delangle, Aurelien Deniaud, et al.

Environmental Science Nano

PAPER

View Article Online
View Journal | View Issue

Cite this: *Environ. Sci.: Nano*, 2018, 5, 1911

Insights into polythiol-assisted AgNP dissolution induced by bio-relevant molecules†

Marianne Marchioni, [a] Thomas Gallon,[ab] Isabelle Worms, ‡[a] Pierre-Henri Jouneau,[c] Colette Lebrun,[b] Giulia Veronesi, [a] Delphine Truffier-Boutry, [d] Elisabeth Mintz,[a] Pascale Delangle, [b] Aurélien Deniaud *[a] and Isabelle Michaud-Soret *[a]

The widespread use of silver nanoparticles (AgNPs) as biocides in consumer products raises concerns about their toxicity to humans and their environmental impact. The biocidal activity is mediated by the release of Ag(I). However, this metal ion is universally toxic to living organisms. For instance, Ag(I) tightly binds to thiol functional groups that are abundant and essential to any cell type. The first intracellular source of thiol, glutathione, is crucial for the control of the redox balance of cells. Dissolution studies using monothiol-containing biomolecules such as glutathione or cysteine provided controversial results, while the impact of polythiol molecules on AgNP behavior remains unexplored. In order to gain insights into polythiol-assisted AgNP dissolution at constant and equal thiol : Ag molarity, we studied the impact of glutathione, phytochelatins with 2, 3 or 6 thiols, and copper chaperone Atx1 and its metal binding site mimic P^2, both containing 2 pre-oriented thiols to chelate Cu(I). The AgNP behavior was monitored by various complementary physicochemical approaches. We demonstrated unambiguously that, under aerobic conditions, these molecules favor AgNP dissolution into Ag(I) ions with a rate that increases with the number of thiols per molecule as well as with their pre-orientation. We also observed that AgNP dissolution into Ag(I) soluble species occurs progressively for the whole AgNP population. This work highlights how transformations of AgNPs are triggered by biomolecules and lays the basis for a deeper understanding of their fate in biological/environmental systems.

Received 23rd March 2018,
Accepted 6th June 2018

DOI: 10.1039/c8en00340h

rsc.li/es-nano

Environmental significance

Silver nanoparticles (AgNPs) are increasingly used as biocides in commercial products but their impact on human health and the environment remains puzzling. AgNP toxicity is mainly based on the release of bioavailable Ag(I) species. AgNPs are subject to other transformations during their life cycle and a comprehensive understanding of nanoparticle fate is required for their safer use. It has already been shown that monothiol molecules can induce either AgNP dissolution or agglomeration, while polythiols have not been studied so far. Bio-relevant polythiols from plants or mammals were shown to favor AgNP dissolution into Ag(I) ions at increasing rates with the number of thiols per molecule and their pre-orientation. This work added some clues for a better understanding of AgNP fate in biological/environmental systems.

1. Introduction

Silver nanoparticles (AgNPs) are the most used nanomaterial in terms of number, as they are present in 25 to 30% of the products declared to contain nanomaterials.[1–3] AgNPs are used as biocides in textiles, food packaging and medical devices such as catheters or wound dressings.[4,5] The biocidal activity is due to the high toxicity of Ag(I) ions that are released from AgNPs.[6] This process is driven by AgNP oxidative dissolution,[7] which requires both oxygen and protons *in vitro*. Three forms of Ag co-exist in aqueous solution: Ag(0) in the NP core, Ag(I) in solution and Ag(I) bound to the NP surface.[7,8]

AgNPs can thus be considered as a reservoir of Ag(I) for long-lasting biocidal effects in the product of interest and

[a] *Univ. Grenoble Alpes, CNRS, CEA, BIG-LCBM, 38000 Grenoble, France. E-mail: aurelien.deniaud@cea.fr, isabelle.michaud-soret@cea.fr; Tel: +33 (0)4 38 78 96 51, +33 (0)4 38 78 99 40*
[b] *Univ. Grenoble Alpes, CEA, CNRS, INAC, SYMMES, F-38000 Grenoble, France*
[c] *Univ. Grenoble Alpes, CEA, INAC-MEM, 38000 Grenoble, France*
[d] *Univ. Grenoble Alpes, CEA, LITEN/DTNM/SEN/L2N, F-38054 Grenoble Cedex 09, France*

† Electronic supplementary information (ESI) available. See DOI: 10.1039/c8en00340h

‡ Present address: Department F.-A. Forel for Environmental and Aquatic Sciences, University of Geneva, 66 boulevard Carl Vogt CH-1211 Geneva 4.

their action is due to the progressive silver ion leaching from the NP surface under aerobic conditions.[8] Molleman *et al.* developed a theoretical model showing that the Ag(I) release in solution is due to oxidative dissolution of OH-bonded surface Ag(I), while it is blocked by the penetration of oxygen radicals into the metallic lattice followed by the formation of stable Ag_6O octahedra involving the first two atomic layers of the NPs.[9] The interplay between these two phenomena was shown to account for numerous empirical observations, such as the pH dependency of ion release and the stabilizing effect of excess Ag(I) on AgNPs in solution.[7,9,10] This model is consistent with experimental data showing that low pH and the presence of oxidants favor AgNP dissolution into ions,[11,12] while chloride is more protective of the NP form[12] as it promotes AgNP agglomeration.

During their life cycle, AgNPs are dispersed in the environment where they are subjected to various transformations. Organisms such as bacteria, plants or animals are thus exposed to several Ag species with different toxic potentials. In soil and wastewater, as has also recently been observed in plants[13] and in mammals,[14] the main transformation described for AgNPs is sulfidation.[15–17] This process has been extensively studied and leads to surface passivation that limits Ag(I) bioavailability and therefore toxicity.[15,18] Studies performed with mammalian cell models showed that AgNPs are endocytosed and further dissolved inside endosomes and lysosomes into Ag(I) soluble species that distribute throughout the cell.[19,20] The kinetics of AgNP dissolution depends on the cell type,[20–22] but as observed *in vitro* it is favored by the lysosomal pH decrease. Intracellular Ag(I) species become coordinated by thiol-containing biomolecules, mainly glutathione (GSH) and metallothionein (MT), which are important actors in cellular metal ion homeostasis.[20–23] These results suggest that Ag(I) might replace Cu(I) or Zn(II) in their native binding sites, in agreement with the fact that thiolates are soft bases that bind tightly to soft acids such as Ag(I) or Cu(I), and with our recent description of Ag(I) coordination to thiol biomolecules and their chemical mimics *in vitro*.[24] Although there is no evidence showing the direct involvement of thiol-containing molecules in the intracellular dissolution of AgNPs, several studies described the interaction of thiol-containing biomolecules with AgNPs *in vitro*. Most of them focused on the simplest and biologically abundant molecules, cysteine and GSH that contain only one thiol.[12] These molecules have a dual behavior: they foster AgNP dissolution at low concentrations, whereas higher concentrations induce agglomeration that prevents dissolution.[12,25–28] Interestingly, some pioneering works also showed that proteins with Cu-binding sites containing at least one exposed thiol trigger AgNP dissolution into ions. In the case of MT, the dissolution is massive and an amorphous Ag–MT structure has been observed *in vitro*,[29] while in the case of azurin it has been evidenced that the redox properties of this protein favor surface Ag oxidation and the subsequent Ag(I) release from the NPs.[29,30]

Nonetheless, the impact of molecules with multiple thiols on the AgNP behavior remains unexplored, although they are produced by living organisms and offer a wide diversity in terms of the number of thiols as well as the molecular architecture. For instance, plants are able to synthesize GSH linear polymers, named phytochelatins (PC, also named class III metallothioneins) bearing between 2 and 11 thiols,[31,32] which are involved in metal detoxification and alternatively proposed to be involved in metal homeostasis in plants.[33,34] PC production can be induced by metal stress including Ag(I), and PCs are able to bind Ag(I).[35] In order to understand the mechanisms involved in thiol-assisted AgNP dissolution and therefore to predict AgNP fate in the presence of polythiol molecules, we analyzed this process using biomolecules as well as chemical mimics with various numbers of thiols per molecule and different chemical architectures. We worked in equal Ag : S molarity in order to rule out the dependency on the stoichiometric ratio and investigate the influence of the scaffold geometry, thiol function orientation and chelation properties on the dissolution. We chose a series of linear thiol-containing biomolecules, GSH and phytochelatin2 (PC2), PC3 and PC6 that possess 1, 2, 3 and 6 thiols, respectively. We also used Atx1, a eukaryote copper chaperone, and its metal binding site mimic P^2, both containing 2 thiols pre-oriented to chelate Cu(I).[36] A combination of methods was used to study the behavior of citrate-coated AgNPs in solution in the presence of these molecules. We found that the higher the number of thiols on a linear backbone, the faster the AgNP dissolution rate. Besides, the comparison of the different molecules having two thiols demonstrated that their pre-orientation as tight metal binding sites increases the AgNP dissolution rate and thus highlights that the chelate effect favors AgNP dissolution.

2. Materials and methods

2.1. Chemicals

20 nm citrate-coated AgNPs were purchased from NanoComposix (20 nm citrate BioPure™ silver), GSH was purchased from Sigma and PC2, PC3 and PC6 were purchased from Eurogentec. The synthesis and characterization of the cyclodecapeptide P^2 ligand were previously described.[36] P^2, GSH, PC2, PC3 and PC6 were resuspended in 10 mM HEPES buffer at pH 7.4.

2.2. Production of Atx1

Atx1 was produced as described previously.[24,37] After purification, Atx1 was aliquoted in 40 mM MES buffer, 400 mM NaCl and 10% glycerol, pH 6, flash frozen in liquid nitrogen and stored at −80 °C. Before AgNP dissolution experiment, Atx1 buffer was exchanged to 10 mM HEPES (pH 7.4) on Nap5 and Nap10 columns (GE-Healthcare). The protein concentration was determined by measuring the absorbance of the Atx1 solution at 280 nm (ε = 5625 M^{-1} cm^{-1}).

2.3. AgNP dissolution kinetics

Prior to each experiment, the concentration of the stock solution of the ligand was determined by free thiol measurement

with Ellman's procedure using 5,5′-dithiobis-2-nitrobenzoic acid. Each free thiol group yields 1 equivalent of 5-thio-2-nitrobenzoic acid (ε_{412nm} = 14 500 M^{-1} cm^{-1}).[38]

For dissolution experiments, AgNPs were diluted to 370 μM Ag in HEPES–citrate buffer (10 mM HEPES, 2 mM sodium citrate pH 7). The ligands were added in order to obtain a final concentration of 370 μM thiol functions. The solutions were then incubated at 24 °C, under 400 rpm agitation for the desired incubation time before Ag quantification and AgNP surface plasmon resonance (SPR) signal or dynamic light scattering (DLS) measurements. The list of samples used and their final concentrations are reported in Table S1.†

Experiments under anaerobic conditions were performed in a glove box (Jacomex), with residual oxygen concentration of 0.05 ppm. The SPR signal was measured with an Uvikon XL spectrophotometer connected to the glove box with an optical fiber.

2.4. Separation of AgNPs and Ag(I) species and silver quantification by ICP-AES

At each time-point, 500 μL of AgNP/ligand solutions were loaded on top of a 100 μL cushion of 0.7 M sucrose before centrifugation at 21 000*g* for 1 h at 20 °C. The supernatant containing soluble Ag(I) species was carefully recovered. Supernatants and pellets were digested in closed tubes overnight at 50 °C by addition of HNO_3 to a final concentration of 25% for the supernatant and a final concentration of 55% for the pellet. Ag was then quantified in each fraction by inductively coupled plasma atomic emission spectroscopy (ICP-AES) using a Shimadzu ICPE-9800.

The dissolution process follows first-order kinetics that can be mathematically described by the equation:

$$[\%\ \text{dissolved Ag(I)}]_t = [\%\ \text{dissolved Ag(I)}]_{\text{total}} \cdot (1 - \exp^{-k_{\text{app}}t})$$

In order to determine the pseudo first-order rates (k_{app}) the ln(% of remaining AgNPs) was plotted as a function of time. Linear regressions were performed between 0 and 4 hours for the different kinetics except for PC6 where it was done between 0 and 3 hours. The slopes were thus $-k_{app}$ in h^{-1} for the dissolution kinetics in the presence of the different molecules.

2.5. AgNP SPR signal and DLS measurements

At the desired time-point, the sample was diluted five times in HEPES–citrate buffer and transferred to a quartz cell. The SPR signal of AgNPs was monitored by recording UV-visible absorbance spectra between 600 and 250 nm on a Shimadzu UV 1800 spectrophotometer. DLS measurements were carried out at 25 °C in a UVette (Eppendorf) on a Nanostar instrument (Wyatt) (detailed information is given in the ESI†).

2.6. Scanning transmission electron microscopy

2.6.1. Grid preparation and imaging. 5 μL of the sample was directly deposited onto a nickel grid coated with a carbon film (mesh 300, Agar Scientific/S160 N3). The drop was then dried in air. Scanning transmission electron microscopy (STEM) micrographs were taken on a Zeiss MERLIN microscope operated at 30 kV, using a solid-state bright-field detector.

2.6.2. STEM micrograph analysis. Micrographs were analyzed in Fiji software.[39] For each sample, the diameters of at least 100 individual NPs were measured. The size distribution was plotted and average diameters and standard deviations were determined in mass function.

2.7. AF4-UVD-MALLS-ICP-MS measurement

Asymmetrical flow field-flow fractionation measurements were conducted on GSH, P^2 and Atx1 containing samples as fully described recently in ref. 40 and in the ESI.† Briefly, a metal free HPLC (1260 Infinity, Agilent Technologies, Santa Clara, USA) was used to inject 50 μL of samples that were pre-diluted 20 times in 10^{-4} M NaOH solution (pH 10) which was also used as an eluent for the separation of the nanoparticles inside the trapezoidal channel (Wyatt Technology, Goleta, USA). The Ag elemental content was analyzed on-line thanks to an inductively coupled plasma mass spectrometer (ICP-MS 7700×, Agilent Technologies). A UV detector (UVD) and multi-angle laser light scattering (MALLS) instrument were used here as online indicators of the presence of AgNPs and their potential dissolution or aggregation, respectively.

3. Results and discussion

3.1. Kinetics of AgNP dissolution into Ag(I) soluble species

In order to analyze AgNP dissolution into Ag(I) species, time-course experiments were performed over 24 hours. The amount of released Ag(I) increased over time in the presence of GSH under conditions with an equimolar amount of Ag and sulfur (S) (Fig. 1A). In order to assess the importance of the amount of thiol in the AgNP dissolution process, the same experiment was performed in the presence of a double amount of GSH in the reaction mixture. A similar rate of Ag(I) release was observed with the two different amounts of GSH during the 24 hour kinetic experiment (Fig. S1†). The use of an equimolar amount of thiol functions in the reaction therefore did not limit the AgNP dissolution process, probably because of the excess of thiols with respect to surface silver atoms already in the 1 : 1 sample. A one to one Ag : S ratio was thus selected for further experiments.

All the tested molecules induced the time-dependent release of Ag(I) (Fig. 1). The rate of Ag(I) release is faster during the first 1 to 2 hours followed by a slower and continuous Ag(I) release. Finally, the dissolution tended to slowly reach a plateau between 10 and 24 hours of incubation, most markedly for P^2 and PC6. This trend has been observed also in previous dissolution studies, and was explained as the simultaneous effect of the formation of insoluble AgO species involving the first two atomic layers of AgNPs and of the increased Ag(I) concentration in solution that stabilized the otherwise labile AgOH species.[9,10,41]

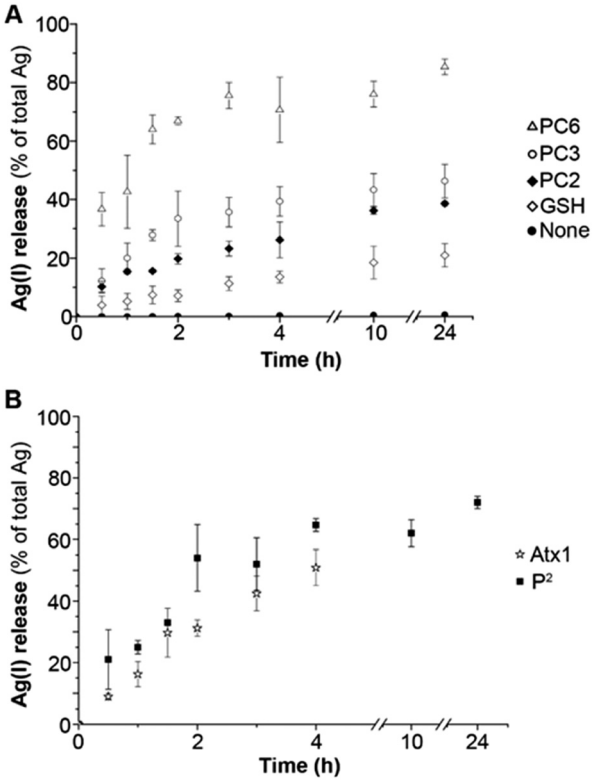

Fig. 1 AgNP dissolution into Ag(I) species in the presence of thiol-containing molecules. Time-dependent measurement of the fraction of Ag(I) released from AgNPs determined by ICP-AES in the presence of GSH, PC2, PC3 and PC6 (A), and P^2 and Atx1 (B). The fraction of Ag(I) released corresponds to the amount of Ag recovered in the supernatant of the sucrose centrifugation divided by the total amount of Ag recovered in both fractions (supernatant + pellet).

AgNP dissolution into Ag(I) follows first order kinetics and pseudo first-order rate constants were determined in order to compare the reaction induced by the different molecules (Table 1). The comparison of the molecules that contain different numbers of thiol functions on a linear backbone GSH, PC2, PC3 and PC6 showed an increase in the initial dissolution rate with the increase of thiols per molecule (Table 1) leading to more than 10-fold faster AgNP dissolution for PC6 compared to that for GSH. Furthermore, the maximal amount of released Ag(I) (Fig. 1A) also correlates with the number of thiol functions present in the molecules reaching 85%, 46%, 39% and 21% for PC6, PC3, PC2 and GSH, respectively. The two thiol functions in PC2 are incorporated on a linear backbone, while the cyclodecapeptide P^2 bears two sulfur atoms pre-oriented to form a tight metal binding site, mimicking the Cu binding loop in the protein Atx1. P^2 analysis showed a more than three times faster initial AgNP dissolution rate (Table 1) and the maximal dissolution after 24 h doubled compared to PC2 (Fig. 1A and B) that contained the same amount of thiols per molecule. These results highlight the importance of thiol pre-orientation on AgNP dissolution. The influence of the protein backbone has been assessed using Atx1 that inspired the molecule P^2. Atx1 showed a slightly slower dissolution rate than P^2 as well as a slightly lower maximal dissolution (Fig. 1B and Table 1). However, these results are based on the fraction of recovered Ag that is lower than the initial amount present in the reaction in the case of Atx1. Indeed, Atx1 also favors AgNP agglomeration that partly sticks to plastic tubes leading to a partial loss of matter. Therefore, the slight difference between P^2 and Atx1 can be due either to this agglomeration phenomenon or to the protein backbone of Atx1 that would lower AgNP dissolution.

Table 1 AgNP dissolution rate (k_{app}) for the first hour of incubation of AgNPs with thiol-containing molecules (average of at least 3 independent experiments)

Molecule	k_{app} (h^{-1})	r^2	Number of thiol groups per molecule
None	0.001	0.85	—
GSH	0.034	0.96	1
PC2	0.068	0.89	2
PC3	0.121	0.89	3
PC6	0.461	0.94	6
P^2	0.249	0.92	2
Atx1	0.179	0.99	2

3.2. Evolution of the AgNP SPR signal in the presence of thiol molecules

As noble metal NPs, AgNPs show a characteristic SPR signal with a maximum at 400 nm. This phenomenon occurs when the frequency of photons matches the natural frequency of surface electrons oscillating against the restoring force.[42] The intensity of the AgNP SPR signal and the wavelength of its maximum give information about the amount of AgNPs in solution, their agglomeration state and their coating.[43] In the case of purely monomeric AgNPs, the evolution of the intensity of the SPR peak around 400 nm enables monitoring the kinetics of AgNP dissolution into Ag(I) species. The AgNP SPR signal intensity decreased over time in the presence of GSH with a faster rate in the first 1.5–2 hours (Fig. 2A and B). PC2, PC3 and PC6 induced a time-dependent decrease of the SPR peak with a rate that increased with the number of thiol functions per molecule (Fig. 2B and S2A–C†). The extent of the SPR signal intensity decrease after 24 hour incubation was also higher with a higher number of thiols per molecule. It reached 68%, 43%, 36% and 18% of the initial absorbance at 400 nm with GSH, PC2, PC3 and PC6, respectively. Furthermore, in all the cases the kinetics of dissolution have the same profile with a faster decrease rate in the first 1.5 hours followed by a slower decrease rate and reached a plateau for PC6.

The behavior of AgNPs in the presence of P^2 and Atx1 was compared with that of PC2 in order to analyze the importance of the thiol function pre-orientation and protein backbone on AgNP dissolution and/or agglomeration mechanisms. In the presence of Atx1, in less than 15 minutes, the SPR signal at 400 nm almost completely disappeared (5% of the signal remaining), a broad peak appeared with a

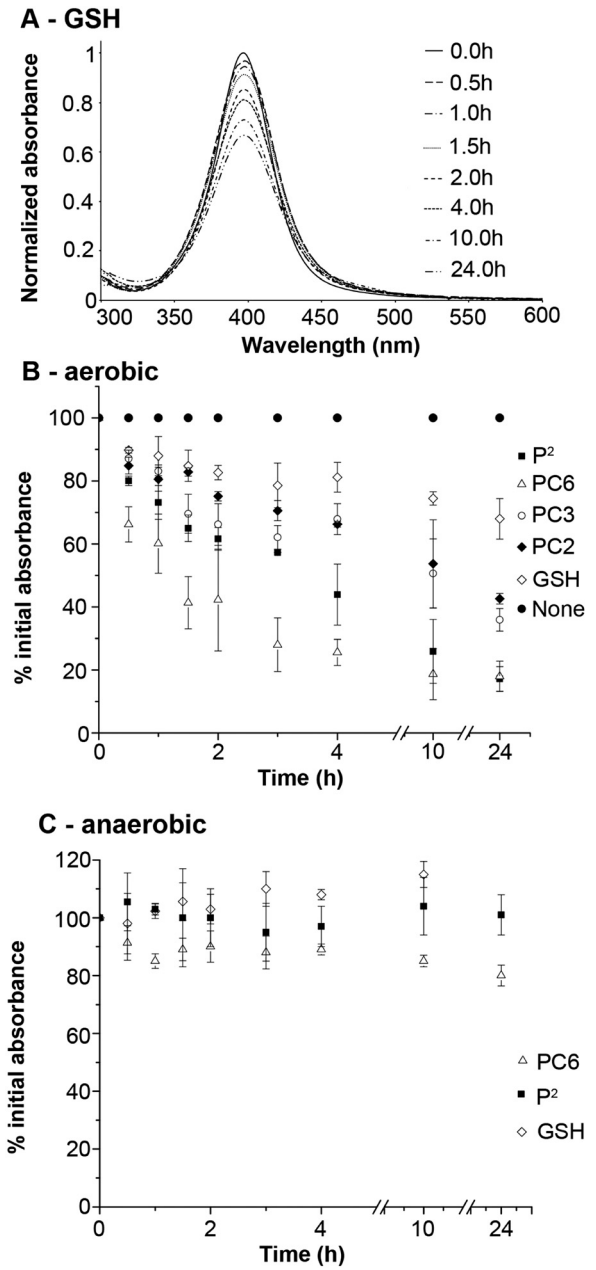

Fig. 2 AgNP SPR signal intensity analysis in the presence of thiol-containing molecules. A) Time-dependent analysis of AgNP SPR spectra in the presence of GSH between 0 and 24 hour incubation. B) Time-dependent analysis of SPR peak intensity in the presence of GSH, P^2, PC2, PC3 and PC6 under aerobic conditions. C) Time-dependent analysis of AgNP SPR peak intensity in the presence of GSH, P^2 and PC6 under anaerobic conditions.

maximum around 550 nm (Fig. S3A†) and large agglomerates can be visually observed in the tube. Altogether, the data showed that Atx1 rapidly led to the massive agglomeration of citrate-coated AgNPs. By contrast, the cyclodecapeptide P^2 only induced the time-dependent decrease of the 400 nm AgNP SPR peak (Fig. 2B and S3B†), suggesting no AgNP agglomeration or aggregation. Interestingly, the decrease of the AgNP SPR peak was significantly faster with P^2 than with PC2 and reached an 82% decrease of the initial absorbance after 24 hour incubation (Fig. 2B and S3B†). These results confirm that the thiol group pre-orientation favors AgNP dissolution under aqueous aerobic conditions. Therefore, except for Atx1, elemental quantification (Fig. 1A and B) and SPR analysis (Fig. 2B) are consistent and prove that AgNPs become dissolved into Ag(I) soluble species in the presence of thiol-containing molecules.

The evolution of the AgNP SPR signal intensity in the presence of some of these molecules was also studied under anaerobic conditions in order to assess the influence of oxygen on the previously observed phenomenon. For these experiments GSH, P^2 and PC6 were selected in order to keep a diversity of molecules in terms of the number of thiols and architectures. In the case of GSH and P^2 no significant decrease in the AgNP SPR signal was observed (Fig. 2C). A slight decrease of the signal appeared within the first hour of incubation of AgNPs with PC6. The normalized optical density decreased rapidly from 1 to 0.8 and then remained stable up to 24 hours of incubation. This decrease may most probably be due to surface effects induced by the AgNP coating by PC6. Altogether, these data show that oxygen is strictly required for thiol-assisted AgNP dissolution. Hypoxic conditions may thus slow down Ag(I) dissolution from AgNPs, while oxidative stress and reactive oxygen species may increase the rate of silver oxidation and Ag(I) release. Altogether, one can suggest that only oxygen is required for AgNP dissolution and then further chemical environments strongly catalyze this process, such as protons and/or thiols.

3.3. Evolution of AgNP diameter in the presence of thiol molecules

In order to monitor the diameter of the particles themselves, *i.e.* the silver core only, STEM analysis was performed (Fig. 3, S4† and Table 2).

The size distributions of AgNPs following 24 hour incubation with GSH, P^2 or PC6 were determined (Fig. 3 and Table 2). These experiments enabled the comparison of ligands leading to fast or slow AgNP dissolution, GSH *versus* P^2 and PC6. Pristine AgNPs had an average diameter of 20 ± 5 nm. The incubation of citrate-coated AgNPs with P^2 or PC6 leads to a better dispersion of the NPs on the grid most probably due to the high affinity coating that replaces citrate and thus avoids AgNP agglomeration during grid preparation (Fig. S4A *versus* C and D†), particularly for P^2 that leads to purely monodisperse AgNPs on the grid. The incubation with the three molecules also decreased the dispersion of the AgNP size distribution (Fig. 3 and Table 2). In the case of GSH, the smallest AgNPs (up to 11 nm) almost completely disappeared and the largest ones were only slightly dissolved (Fig. 3 and S4B†), leading to a diameter of 19 ± 3 nm. This result showed that AgNP dissolution induced by thiol-containing molecules does not occur at the same rate for AgNPs of different diameters, with the smallest being dissolved faster and/or preferentially. In the case of P^2 and

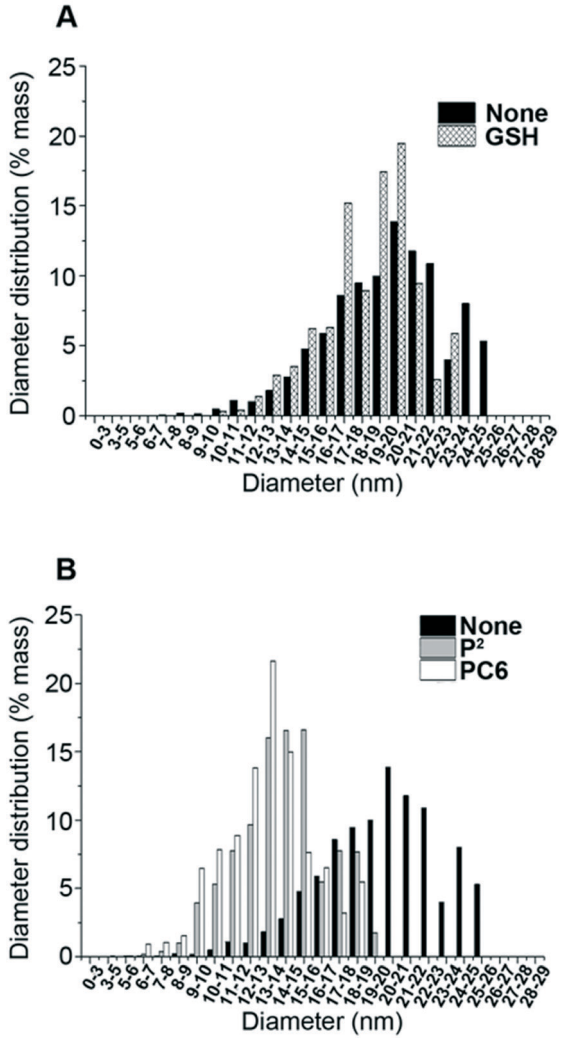

Fig. 3 AgNP size distribution in the presence of thiol-containing molecules. Histograms of AgNP diameters measured from STEM micrographs of input AgNPs and AgNPs with GSH after 24 hour incubation (A), and pristine AgNPs and AgNPs with P^2 or PC6 after 24 hour incubation (B).

PC6, 24 hour incubation with AgNPs induced a significant decrease of their size, leading to diameters of 15 ± 3 nm and 14 ± 3 nm for P^2 and PC6, respectively (Fig. 3 and S4C and D†).

In order to corroborate our results, we calculated the average NP diameters expected after 24 hour incubation starting from the dissolution values measured by ICP-AES (Fig. 1), and compared them to the diameters measured by STEM (Table 2).

We considered a purely monodisperse AgNP stock solution of 20.2 nm in diameter, the average size of the AgNP population. The expected NP diameter d corresponding to the percentage of dissolution experimentally determined by ICP-AES was calculated. In the simplest case of uniform dissolution, the volume V of the partially dissolved NPs can be written as:

$$V = \frac{1}{6}\pi d^3 = x\frac{m}{\rho} \quad (1)$$

where m is the mass of a pristine AgNP, ρ is the density of Ag metal that can be assumed to be applicable for nanoparticulate Ag(0) (ρ_{Ag} = 10.5 g cm^{-3}), and x is the fraction of undissolved NPs. The expected diameter d was thus calculated as:

$$d = \sqrt[3]{\frac{6xm}{\pi\rho}} \quad (2)$$

The diameters calculated on the basis of the fraction of dissolution determined by ICP-AES are in agreement within the errors with the average diameters determined from STEM micrographs (Table 2). However, the calculated diameters are smaller than the average values determined by STEM, particularly for the small size NPs. This is probably due to the fact that surface effects become overriding with very small AgNPs since the external AgO layer is non-negligible and less dense than the Ag(0) core. Besides, in mass the diameter distribution is not Gaussian, probably affecting the precision of the calculation.

The influence of different thiol-containing molecules on the AgNP diameter and size distribution was also monitored by DLS (Table 2). This method is complementary to STEM analysis, since DLS provides the hydrodynamic diameter that is indicative of both the core of the NPs as well as their coating. Therefore, the hydrodynamic diameter changes depend not only on AgNP dissolution but also on the size and the extent of binding of the coating molecule. Moreover, DLS is

Table 2 AgNP size in the presence of thiol-containing molecules. AgNP core diameter determined by STEM, theoretical diameter based on ICP-AES results and hydrodynamic diameter and polydispersity index obtained by DLS of input citrate-coated AgNPs and following a 24 hour incubation with the different thiol molecules

Ligand	AgNP core diameter determined by STEM (nm, from distribution in mass)	Theoretical diameter calculated based on ICP-AES AgNP dissolution results (nm)	Hydrodynamic diameter (nm) measured by DLS (mass) after 24 h incubation (polydispersity index)	Molecular weight of the molecules (Da)
None	20.2 ± 4.9 at t0	20.2	24.8 (16%) at t0	—
GSH	19.1 ± 3.1	18.8 ± 0.3	23.2 (12%)	307
PC2	—	17.1 ± 0.1	20.8 (16%)	540
PC3	—	16.4 ± 0.5	20.6 (10%)	773
PC6	13.7 ± 3.3	10.5 ± 0.5	18.5 (9%)	1469
P^2	14.5 ± 3.1	11.8 ± 0.6	18.7 (7%)	1090

performed in solution and the PDI gives information on the homogeneity of the sample in solution such as signs of agglomeration. The initial particles had a hydrodynamic diameter of 24.8 nm and a polydispersity index (PDI) of 16% (Table 2). These values are higher than expected and this is most probably due to a slight agglomeration of the NPs. This is confirmed by the results obtained with the different thiol molecules that coat the NPs, stabilizing them, resulting in monodispersity and thus decreasing their PDI (Table 2) as already observed on STEM grids (Fig. S4†). The measurements after 24 hour incubation showed a decrease in hydrodynamic diameter with all the molecules leading to diameters ranging between 18.5 and 23.2 nm (Table 2). The differences between the molecules appeared limited and did not reflect the extent of AgNP dissolution measured by ICP-AES (Fig. 1). However, taking into account the molecular weight of the ligands (Table 2), in particular for P^2 and PC6, and their high affinity for AgNPs, one can easily assume a much larger coating layer compared to GSH, for instance. This may explain the minimal decrease in the hydrodynamic diameter with P^2 and PC6. Therefore, a combined STEM/DLS analysis provides complementary information.

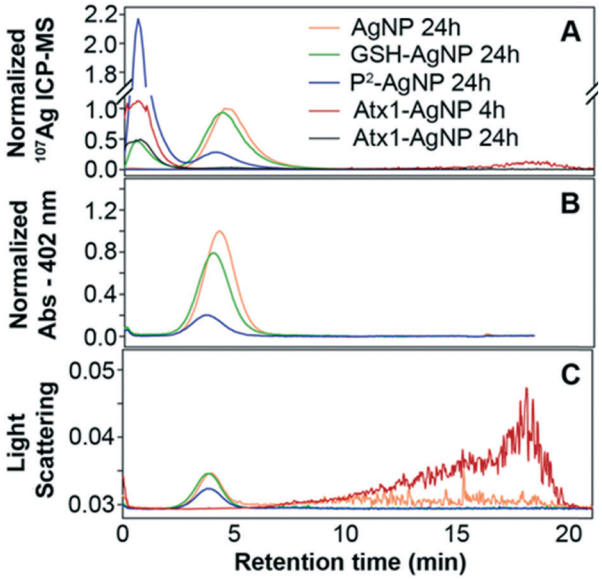

Fig. 4 AF4 analysis of AgNPs in the presence of GSH, P^2 and Atx1. Fractograms of species from AgNPs incubated with GSH and P^2 for 24 hours and with Atx1 for 4 hours and 24 hours. The detection is based on ^{107}Ag by ICP-MS (A); absorbance at 402 nm (B) and light scattering (C).

3.4. Progressive AgNP dissolution in the presence of thiol-containing molecules

AF4-UVD-MALLS-ICP-MS experiments were performed in order to separate the different species according to their hydrodynamic sizes after incubation of AgNPs with GSH, P^2 and Atx1. By minimizing sample handling, this method enables obtaining an integrated multi-parameter measurement that gives an overview of the AgNP colloidal state and dissolution. Without a ligand, AgNPs are eluted at a retention time of 4.7 minutes (Fig. 4A). In the presence of GSH and P^2, Ag eluted in 2 peaks after 24 hours of incubation. The first peak had a low retention time around 0.6–0.8 minutes without any specific absorbance of AgNPs and should correspond to Ag(I) bound to the thiol molecules (Fig. 4B). The second Ag peak had a retention time around 4.4 and 4.2 minutes for GSH and P^2, respectively, and was associated with an absorbance signal at 402 nm. Therefore, both GSH- and P^2-coated AgNPs eluted before citrate-coated AgNPs. These minute changes in retention behavior can be attributed to the change in AgNP hydrodynamics due to coating exchanges, leading to a better dispersion as already pointed out by DLS and STEM, or due to lower interactions with the membrane. However, under our elution conditions, retention times could hardly be directly related to changes in AgNP primary sizes.[40] The difference in the absorbance intensity of AgNP peaks is coherent with a decrease in AgNP content when GSH or P^2 are present. Indeed, the amount of Ag associated with AgNP peaks corresponds to ~85% of the initial total Ag for GSH–AgNPs and ~30% for P^2–AgNPs after 24 hour incubation. These results are consistent with the results obtained by ICP-AES measurements (Fig. 1), for which the Ag release from AgNPs was found to be ~20% and ~70% in the presence of GSH and P^2, respectively. In the case of Atx1, the fractograms clearly show an almost complete disappearance of individual AgNPs but a residual Ag signal is observed at high retention times (between 15 and 20 minutes), after only 4 hours of incubation (Fig. 4A). In addition, a broad peak of Ag(I)–Atx1 species was also present at 1–2 minutes retention time but its intensity decreased between 4 and 24 hour incubation times reflecting the loss of material due to adhesion to the plastic tube (Fig. 4A). The high intensity of scattered light observed at the end of the elution (Fig. 4C) supports the formation of AgNP heterogeneous aggregates in the presence of Atx1 for a still unknown reason. This phenomenon thus shows that a protein backbone can affect the interaction with AgNPs and influence their behavior in solution, independent of the dissolution. This agglomeration-prone effect can decrease the AgNP dissolution extent as has already been described with cysteine that does not induce AgNP dissolution but a kind of passivation mechanism.[10] Other one-thiol molecules have been described to protect AgNPs by forming a tight comb-like coating.[8,44] Therefore, there is a diversity of AgNP reactivity in the presence of thiol-containing molecules which depends on the molecular "scaffold" and which remains difficult to predict.

Altogether, our AF4-UVD-MALLS-ICP-MS data confirmed the trends in the AgNP dissolution process drawn based on other results. Particularly, the combined analysis of STEM, DLS and AF4-ICP-MS data showed a progressive and global decrease of the average diameter of AgNP species in the presence of thiol molecules. Indeed, fairly homogeneous AgNP populations are observed upon thiol-assisted dissolution. The profiles of the AgNP diameter distributions are thus similar all throughout the dissolution process with all AgNPs decreasing in size, which shows that the dissolution occurs

progressively on all AgNPs leading to a decrease in the average diameter and not in the dispersion (Fig. 3). In the case of GSH, the population of smaller AgNPs dissolved preferentially. We managed to catch this event thanks to the slow dissolution in the presence of GSH. This phenomenon probably occurs on a time scale different from the ones we explored with the other thiolate molecules. These results are consistent with the literature that describes a higher extent of dissolution of the smallest AgNPs into Ag(I) species both in water and in acid pH aqueous media.[11] Therefore, whether the oxidative dissolution mechanism in place is proton- or thiol-catalyzed, the smallest AgNPs are preferentially dissolved into Ag(I) species.

4. Conclusions

In this work, we analyzed in detail the AgNP behavior in the presence of a series of molecules containing thiol functional groups. The experiments have been performed in equimolar amounts of Ag and S regardless of the molecule and its ability to bind Ag(I). Indeed, some molecules have a higher tendency to coordinate Ag(I) with 2 sulfur atoms, while others favor 3 sulfur coordination. The analysis of linear molecules containing up to 6 thiol functions showed that the higher the number of thiols, the faster the AgNP dissolution. We also compared different molecules with 2 thiols and found that the pre-orientation of the thiol triggered a chelate effect that increased the AgNP dissolution rate.

Besides, the dissolution process combined with the agglomeration-prone mechanism observed with Atx1 could be more general for proteins with solvent-exposed thiol groups. Indeed, we recently showed a similar behavior with MT in the presence of citrate-coated AgNPs.[29] In this case, MT induced the formation of amorphous Ag–MT species of large size observed by TEM. Besides, Ag–S rich amorphous structures have already been observed in mammalian cells exposed to AgNPs.[45] The biomolecules located in these structures have not been identified but the most prominent intracellular thiol-containing molecules following AgNP exposure are GSH and MT.[20–23] Therefore, one can imagine that the phenomenon observed *in vitro* with Atx1 and MT is similar to what happens inside cells. However, it is not possible to know whether these precipitate-like structures are less toxic to living cells since they trap Ag(I) species or whether they are a long-lasting reservoir of Ag(I) inside cells that could in addition trigger inflammation mechanisms.

In conclusion, this work brings insight into the AgNP dissolution mechanism induced by polythiol molecules, which can lead to a better understanding of the mechanisms underlying AgNP transformations both in the environment and in various organisms.

Contributions

IMS, AD, PD, EM and MM designed this research; MM, TG and IW carried out the experiments; PHJ performed the STEM experiments; CL synthesized P^2; MM, AD, IMS, IW, PD, TG, GV and DB analyzed the data and AD, MM, IMS, PD and GV wrote the paper.

Conflicts of interest

There are no conflicts to declare.

Acknowledgements

We acknowledge R. Miras for help for Atx1 purification, S Motellier for AF4 experiment support and F. Rollin-Genetet and C. Vidaud for discussion. This work was funded by the CEA-Toxicology Transversal Program through the Nano-SilverSol grant and by the CEA Transversal Programs Toxicology and Nanoscience through the NanoTox-RX grant. This research is part of the LabEx SERENADE (grant ANR-11-LABX-0064) and the LabEx ARCANE (grant ANR-11-LABX-0003-01). MM and IW were supported by the LabEx SERENADE. The AF4-ICP-MS was funded by the EQUIPEX NanoID (grant ANR-10-EQPX-39-01). This work is also supported by the CEA DRF-Impulsion grant FIB-Bio and the Université Grenoble Alpes – AGIR grant NanoSilverSafe.

References

1 R-Nano, https://www.r-nano.fr/?locale=en, web database.
2 M. E. Vance, T. Kuiken, E. P. Vejerano, S. P. McGinnis, M. F. Hochella, Jr., D. Rejeski and M. S. Hull, Nanotechnology in the real world: Redeveloping the nanomaterial consumer products inventory, *Beilstein J. Nanotechnol.*, 2015, **6**, 1769–1780.
3 S. W. P. Wijnhoven, W. J. G. M. Peijnenburg, C. A. Herberts, W. I. Hagens, A. G. Oomen, E. H. W. Heugens, B. Roszek, J. Bisschops, I. Gosens, D. Van De Meent, S. Dekkers, W. H. De Jong, M. van Zijverden, A. J. A. M. Sips and R. E. Geertsma, Nano-silver – a review of available data and knowledge gaps in human and environmental risk assessment, *Nanotoxicology*, 2009, **3**, 109–138.
4 K. Chaloupka, Y. Malam and A. M. Seifalian, Nanosilver as a new generation of nanoproduct in biomedical applications, *Trends Biotechnol.*, 2010, **28**, 580–588.
5 K. Mijnendonckx, N. Leys, J. Mahillon, S. Silver and R. Van Houdt, Antimicrobial silver: uses, toxicity and potential for resistance, *BioMetals*, 2013, **26**, 609–621.
6 A. Ivask, A. Elbadawy, C. Kaweeteerawat, D. Boren, H. Fischer, Z. Ji, C. H. Chang, R. Liu, T. Tolaymat, D. Telesca, J. I. Zink, Y. Cohen, P. A. Holden and H. A. Godwin, Toxicity mechanisms in Escherichia coli vary for silver nanoparticles and differ from ionic silver, *ACS Nano*, 2014, **8**, 374–386.
7 J. Liu and R. H. Hurt, Ion release kinetics and particle persistence in aqueous nano-silver colloids, *Environ. Sci. Technol.*, 2010, **44**, 2169–2175.
8 J. Liu, D. A. Sonshine, S. Shervani and R. H. Hurt, Controlled release of biologically active silver from nanosilver surfaces, *ACS Nano*, 2010, **4**, 6903–6913.
9 B. Molleman and T. Hiemstra, Surface Structure of Silver Nanoparticles as a Model for Understanding the Oxidative

Dissolution of Silver Ions, *Langmuir*, 2015, **31**, 13361–13372.

10 K. Loza, J. Diendorf, C. Sengstock, L. Ruiz-Gonzalez, J. M. Gonzalez-Calbet, M. Vallet-Regi, M. Koller and M. Epple, The dissolution and biological effects of silver nanoparticles in biological media, *J. Mater. Chem. B*, 2014, **2**, 1634–1643.

11 T. S. Peretyazhko, Q. Zhang and V. L. Colvin, Size-controlled dissolution of silver nanoparticles at neutral and acidic pH conditions: kinetics and size changes, *Environ. Sci. Technol.*, 2014, **48**, 11954–11961.

12 L. Sigg and U. Lindauer, Silver nanoparticle dissolution in the presence of ligands and of hydrogen peroxide, *Environ. Pollut.*, 2015, **206**, 582–587.

13 A. E. Pradas Del Real, V. Vidal, M. Carriere, H. Castillo-Michel, C. Levard, P. Chaurand and G. Sarret, Silver Nanoparticles and Wheat Roots: A Complex Interplay, *Environ. Sci. Technol.*, 2017, **51**, 5774–5782.

14 D. A. Gonzalez-Carter, B. F. Leo, P. Ruenraroengsak, S. Chen, A. E. Goode, I. G. Theodorou, K. F. Chung, R. Carzaniga, M. S. Shaffer, D. T. Dexter, M. P. Ryan and A. E. Porter, Silver nanoparticles reduce brain inflammation and related neurotoxicity through induction of H2S-synthesizing enzymes, *Sci. Rep.*, 2017, **7**, 42871.

15 C. Levard, E. M. Hotze, G. V. Lowry and G. E. Brown, Jr., Environmental transformations of silver nanoparticles: impact on stability and toxicity, *Environ. Sci. Technol.*, 2012, **46**, 6900–6914.

16 C. Levard, S. Mitra, T. Yang, A. D. Jew, A. R. Badireddy, G. V. Lowry and G. E. Brown, Jr., Effect of chloride on the dissolution rate of silver nanoparticles and toxicity to E. coli, *Environ. Sci. Technol.*, 2013, **47**, 5738–5745.

17 C. Levard, B. C. Reinsch, F. M. Michel, C. Oumahi, G. V. Lowry and G. E. Brown, Sulfidation processes of PVP-coated silver nanoparticles in aqueous solution: impact on dissolution rate, *Environ. Sci. Technol.*, 2011, **45**, 5260–5266.

18 T. Miclaus, C. Beer, J. Chevallier, C. Scavenius, V. E. Bochenkov, J. J. Enghild and D. S. Sutherland, Dynamic protein coronas revealed as a modulator of silver nanoparticle sulphidation in vitro, *Nat. Commun.*, 2016, **7**, 11770.

19 V. De Matteis, M. A. Malvindi, A. Galeone, V. Brunetti, E. De Luca, S. Kote, P. Kshirsagar, S. Sabella, G. Bardi and P. P. Pompa, Negligible particle-specific toxicity mechanism of silver nanoparticles: the role of Ag+ ion release in the cytosol, *Nanomedicine*, 2015, **11**, 731–739.

20 G. Veronesi, A. Deniaud, T. Gallon, P. H. Jouneau, J. Villanova, P. Delangle, M. Carriere, I. Kieffer, P. Charbonnier, E. Mintz and I. Michaud-Soret, Visualization, quantification and coordination of Ag+ ions released from silver nanoparticles in hepatocytes, *Nanoscale*, 2016, **8**, 17012–17021.

21 X. Jiang, T. Miclăuș, L. Wang, R. Foldbjerg, D. S. Sutherland, H. Autrup, C. Chen and C. Beer, Fast intracellular dissolution and persistent cellular uptake of silver nanoparticles in CHO-K1 cells: implication for cytotoxicity, *Nanotoxicology*, 2014, **9**, 181–189.

22 L. Wang, T. Zhang, P. Li, W. Huang, J. Tang, P. Wang, J. Liu, Q. Yuan, R. Bai, B. Li, K. Zhang, Y. Zhao and C. Chen, Use of Synchrotron Radiation-Analytical Techniques To Reveal Chemical Origin of Silver-Nanoparticle Cytotoxicity, *ACS Nano*, 2015, **9**, 6532–6547.

23 G. Veronesi, C. Aude-Garcia, I. Kieffer, T. Gallon, P. Delangle, N. Herlin-Boime, T. Rabilloud and M. Carriere, Exposure-dependent Ag+ release from silver nanoparticles and its complexation in AgS2 sites in primary murine macrophages, *Nanoscale*, 2015, **7**, 7323–7330.

24 G. Veronesi, T. Gallon, A. Deniaud, B. Boff, C. Gateau, C. Lebrun, C. Vidaud, F. Rollin-Genetet, M. Carriere, I. Kieffer, E. Mintz, P. Delangle and I. Michaud-Soret, XAS Investigation of Silver(I) Coordination in Copper(I) Biological Binding Sites, *Inorg. Chem.*, 2015, **54**, 11688–11696.

25 E. Amato, Y. A. Diaz-Fernandez, A. Taglietti, P. Pallavicini, L. Pasotti, L. Cucca, C. Milanese, P. Grisoli, C. Dacarro, J. M. Fernandez-Hechavarria and V. Necchi, Synthesis, characterization and antibacterial activity against Gram positive and Gram negative bacteria of biomimetically coated silver nanoparticles, *Langmuir*, 2011, **27**, 9165–9173.

26 A. P. Gondikas, A. Morris, B. C. Reinsch, S. M. Marinakos, G. V. Lowry and H. Hsu-Kim, Cysteine-induced modifications of zero-valent silver nanomaterials: implications for particle surface chemistry, aggregation, dissolution, and silver speciation, *Environ. Sci. Technol.*, 2012, **46**, 7037–7045.

27 K. Siriwardana, A. Wang, M. Gadogbe, W. E. Collier, N. C. Fitzkee and D. Zhang, Studying the Effects of Cysteine Residues on Protein Interactions with Silver Nanoparticles, *J. Phys. Chem. C*, 2015, **119**, 2910–2916.

28 K. Afshinnia, I. Gibson, R. Merrifield and M. Baalousha, The concentration-dependent aggregation of Ag NPs induced by cystine, *Sci. Total Environ.*, 2016, **557-558**, 395–403.

29 W. Liu, I. A. M. Worms, N. Herlin-Boime, D. Truffier-Boutry, I. Michaud-Soret, E. Mintz, C. Vidaud and F. Rollin-Genetet, Interaction of silver nanoparticles with metallothionein and ceruloplasmin: impact on metal substitution by Ag(i), corona formation and enzymatic activity, *Nanoscale*, 2017, **9**, 6581–6594.

30 A. J. Martinolich, G. Park, M. Y. Nakamoto, R. E. Gate and K. E. Wheeler, Structural and functional effects of Cu metalloprotein-driven silver nanoparticle dissolution, *Environ. Sci. Technol.*, 2012, **46**, 6355–6362.

31 S. Clemens, E. J. Kim, D. Neumann and J. I. Schroeder, Tolerance to toxic metals by a gene family of phytochelatin synthases from plants and yeast, *EMBO J.*, 1999, **18**, 3325–3333.

32 P. Tennstedt, D. Peisker, C. Bottcher, A. Trampczynska and S. Clemens, Phytochelatin synthesis is essential for the detoxification of excess zinc and contributes significantly to the accumulation of zinc, *Plant Physiol.*, 2009, **149**, 938–948.

33 C. Cobbett and P. Goldsbrough, Phytochelatins and metallothioneins: roles in heavy metal detoxification and homeostasis, *Annu. Rev. Plant Biol.*, 2002, **53**, 159–182.

34 M. Pivato, M. Fabrega-Prats and A. Masi, Low-molecular-weight thiols in plants: functional and analytical implications, *Arch. Biochem. Biophys.*, 2014, **560**, 83–99.
35 R. K. Mehra, K. Tran, G. W. Scott, P. Mulchandani and S. S. Saini, Ag(I)-binding to phytochelatins, *J. Inorg. Biochem.*, 1996, **61**, 125–142.
36 A. M. Pujol, M. Cuillel, O. Renaudet, C. Lebrun, P. Charbonnier, D. Cassio, C. Gateau, P. Dumy, E. Mintz and P. Delangle, Hepatocyte targeting and intracellular copper chelation by a thiol-containing glycocyclopeptide, *J. Am. Chem. Soc.*, 2011, **133**, 286–296.
37 R. Miras, I. Morin, O. Jacquin, M. Cuillel, F. Guillain and E. Mintz, Interplay between glutathione, Atx1 and copper. 1. Copper(I) glutathionate induced dimerization of Atx1, *JBIC, J. Biol. Inorg. Chem.*, 2008, **13**, 195–205.
38 G. L. Ellman, Tissue sulfhydryl groups, *Arch. Biochem. Biophys.*, 1959, **82**, 70–77.
39 J. Schindelin, I. Arganda-Carreras, E. Frise, V. Kaynig, M. Longair, T. Pietzsch, S. Preibisch, C. Rueden, S. Saalfeld, B. Schmid, J. Y. Tinevez, D. J. White, V. Hartenstein, K. Eliceiri, P. Tomancak and A. Cardona, Fiji: an open-source platform for biological-image analysis, *Nat. Methods*, 2012, **9**, 676–682.
40 S. Motellier, N. Pelissier and J. G. Mattei, Contribution of single particle inductively coupled plasma mass spectrometry and asymmetrical flow field-flow fractionation for the characterization of silver nanosuspensions. Comparison with other sizing techniques, *J. Anal. At. Spectrom.*, 2017, **32**, 1348–1358.
41 S. Kittler, C. Greulich, J. Diendorf, M. Köller and M. Epple, Toxicity of Silver Nanoparticles Increases during Storage Because of Slow Dissolution under Release of Silver Ions, *Chem. Mater.*, 2010, **22**, 4548–4554.
42 A. Moores and F. Goettmann, The plasmon band in noble metal nanoparticles: an introduction to theory and applications, *New J. Chem.*, 2006, **30**, 1121–1132.
43 V. Banerjee and K. P. Das, Interaction of silver nanoparticles with proteins: A characteristic protein concentration dependent profile of SPR signal, *Colloids Surf., B*, 2013, **111**, 71–79.
44 F. Porcaro, L. Carlini, A. Ugolini, D. Visaggio, P. Visca, I. Fratoddi, I. Venditti, C. Meneghini, L. Simonelli, C. Marini, W. Olszewski, N. Ramanan, I. Luisetto and C. Battocchio, Synthesis and Structural Characterization of Silver Nanoparticles Stabilized with 3-Mercapto-1-Propansulfonate and 1-Thioglucose Mixed Thiols for Antibacterial Applications, *Materials*, 2016, **9**, 1028.
45 C. Aude-Garcia, F. Villiers, V. Collin-Faure, K. Pernet-Gallay, P.-H. Jouneau, S. Sorieul, G. Mure, A. Gerdil, N. Herlin-Boime, M. Carrière and T. Rabilloud, Different in vitro exposure regimens of murine primary macrophages to silver nanoparticles induce different fates of nanoparticles and different toxicological and functional consequences, *Nanotoxicology*, 2015, 1–11, DOI: 10.3109/17435390.2015.1104738.

